Microelectronics Journal 40 (2009) 309–312

Contents lists available at ScienceDirect

Microelectronics Journal

journal homepage: www.elsevier.com/locate/mejo

Structural and optical properties on thulium-doped LHPG-grown Ta_2O_5 fibres

M. Macatrão [a], M. Peres [a], C.P.L. Rubinger [a], M.J. Soares [a], L.C. Costa [a], F.M. Costa [a], T. Monteiro [a,*], N. Franco [b], E. Alves [b], B.Z. Saggioro [c], M.R.B. Andreeta [c], A.C. Hernandes [c]

[a] Departamento de Física e I3N, Universidade de Aveiro, 3810-193 Aveiro, Portugal
[b] Instituto Tecnológico e Nuclear, 2686-953 Sacavém, Portugal
[c] Instituto de Física de São Carlos, Universidade de São Paulo (USP), C.P. 369, CEP 13560-970, São Carlos, SP, Brazil

ARTICLE INFO

Available online 18 September 2008

Keywords:
Tantalum pentoxide
LHPG-growth
Rare earth doping
XRD
PL

ABSTRACT

Structural, spectroscopic and dielectric properties of thulium-doped laser-heated pedestal Ta_2O_5 as-grown fibres were studied. Undoped samples grow preferentially with a single crystalline monoclinic structure. The fibre with the lowest thulium content (0.1 at%) also shows predominantly a monoclinic phase and no intra-$4f^{12}$ Tm^{3+} recombination was observed. For sample with the highest thulium amount (1.0 at%), the appearance of a dominant triclinic phase as well as intraionic optical activation was observed. The dependence of photoluminescence on excitation energy allows identification of different site locations of Tm^{3+} ions in the lattice. The absence of recombination between the first and the ground-state multiplets as well as the temperature dependence of the observed transitions was justified by an efficient energy transfer between the Tm^{3+} ions. Microwave dielectric properties were investigated using the small perturbation theory. At a frequency of 5 GHz, the undoped material exhibits a dielectric permittivity of 21 and for thulium-doped Ta_2O_5 samples it decreases to 18 for the highest doping concentration. Nevertheless, the dielectric losses maintain a very low value.

1. Introduction

Tantalum pentoxide is a well-known candidate for applications in integrated capacitors for dynamic memories and gate insulators. The high dielectric constant together with other suitable physical properties makes Ta_2O_5 one of the most promising material dielectric alternative to SiO_2 [1–3]. Recent studies showed that the dielectric constant of Ta_2O_5 can be improved through TiO_2 addition, due to stabilization of high-temperature form [4]. This way, a scale down of capacity components will be expected and so with the memory devices.

Besides its interest for electronic devices, its high transparency constitutes one of the major key factors for the use of Ta_2O_5 as optical material for medical and remote atmospheric sensing applications [5]. For these purposes oxide materials are currently doped with rare-earth (RE) ions in order to improve the efficiency of infrared emission. Among these, trivalent thulium ions are known to offer a number of features in this spectral region due to the intra-$4f^{12}$ transitions. In particular, the $^{2S+1}L_J$ manifold transitions $^3F_4 \rightarrow {}^3H_6$ (~1.8 μm), $^3H_4 \rightarrow {}^3F_4$ (~1.5 μm) are of great interest for surgery, optical communications and remote sensing [5].

In the present work, we focus on the structural and optical characterization of Ta_2O_5 undoped and thulium oxide-doped (0.1 and 1 at%) laser heated pedestal growth (LHPG)-grown fibres. The pure and the lowest content doped samples were found to have a monoclinic crystalline structure, while the appearance of a triclinic phase was promoted by higher thulium amounts. Also, the intra-$4f^{12}$ recombination was observed for the highest-doped fibre and from excitation energy and temperature dependence of the observed photoluminescence (PL) a model for the recombination processes is proposed.

2. Experimental

Undoped and Tm_2O_3-doped (0.1 and 1.0 at%) Ta_2O_5 homogeneous pedestals, with 1 mm of diameter and 50 mm of length, were prepared by cold extrusion and dried in air. Crystalline fibres with ~400 μm of diameter were grown by the LHPG technique using a CO_2 laser, as described elsewhere [6]. High-resolution X-ray diffraction experiments were done using a Bruker-AXS D8 Discover diffractometer using the Cu $K_{\alpha 1}$ line in order to be able to distinguish between monoclinic and triclinic phases. Angular $2\theta-\theta$ scans around $(1\,1\,\bar{1}\,0)$ and $(1\,\bar{1}\,1\,0)$ crystallographic planes on undoped and 0.1 at%-doped samples, were performed. For the 1.0 at%-doped samples the scans were performed around $(2\,1\,\bar{1}\,0)$ and $(2\,\bar{1}\,1\,0)$ in order to observe the

* Corresponding author. Tel.: +351 234 370 824; fax: +351 234 378 197.
E-mail address: tita@ua.pt (T. Monteiro).

0026-2692/$ - see front matter © 2008 Elsevier Ltd. All rights reserved.
doi:10.1016/j.mejo.2008.07.033

splitting of the Bragg peaks, an indication of the phase transition from monoclinic to triclinic.

PL measurements were carried out above (He–Cd laser, 325 nm) and below (Ar^+ laser lines) band-gap excitation as reported elsewhere [6]. In the infrared spectral region a Brucker 66 V Fourier-transform spectrometer was used. The signal was detected with a North-Coast EO-817 liquid-nitrogen-cooled-germanium detector.

To measure the complex permittivity of the material, $\varepsilon^* = \varepsilon' - i\varepsilon''$, a cavity perturbation method was used [7], in a rectangular cavity, operating in the $TE_{1,0,11}$ mode, at about 5 GHz. In the centre of the cavity, where the electrical field is maximal, the sample is inserted, provoking the perturbation of the field. According to the small perturbation theory, a linear relationship exists between the frequency shift, Δf, caused by the insertion of a sample in the cavity, and the real part of the complex permittivity of the material, ε'. The same behaviour is observed in the change in the inverse of the quality factor of the cavity, $\Delta(1/Q)$, related to the imaginary part, ε'' [8].

3. Results and discussion

In order to determine the crystalline phase of the undoped and Tm^{3+}-doped LHPG Ta_2O_5 crystalline fibres $2\theta-\theta$ XRD patterns were recorded as shown in Fig. 1a for undoped sample and as in Fig. 1b for the 1.0 at%-doped sample. The XRD Bragg peaks reveal the presence of a dominant monoclinic crystalline structure for the undoped and 0.1 at%-doped fibres. The presence of a single peak around the (1 1 10) and (1 $\bar{1}$ 10) crystallographic planes confirms this conclusion. The presence of other minor phases cannot be ruled out but this would imply the splitting of the diffraction peak. This is the case shown in Fig. 1b which indicates a diffraction pattern of a triclinic phase where the principal directions [1 0 0] and [0 1 0] are not orthogonal, and are responsible for the splitting of the peaks. Again, we cannot rule out the presence of a minor fraction of the monoclinic phase, which signal appears mixed with the triclinic phase.

With a $4f^{12}$ configuration, the energy levels of the Tm^{3+} ion inside the Ta_2O_5 wide band gap (~326 nm at room temperature (RT) as shown in Fig. 2a) correspond to the multiplet manifolds ($^{2S+1}L_J$) $^1G_4$, $^3F_2$, $^3F_3$, $^3H_4$, $^3H_5$, $^3F_4$ and $^3H_6$ [9]. The splitting into Stark components of the free ion levels depends on the RE ion site symmetry on the crystal. With 325 nm excitation, the 14 K PL in the 340–850 nm spectral range for the highest Tm^{3+}-doped sample (the one that shows intraionic recombination) is dominated by the $^3H_4 \rightarrow {}^3H_6$ transition at ~800 nm, as shown in Fig. 2b. Overlapped with the green band, commonly observable in undoped samples, the $^1G_4 \rightarrow {}^3H_6$ transition (~486 nm) is also identified. Under the used excitation conditions the typical $^1G_4 \rightarrow {}^3F_4$ (~650 nm) and $^1G_4 \rightarrow {}^3H_5$ (~780 nm) cannot be detected. Noticed spectral changes occur for a resonant excitation ($\lambda = 476$ nm) into the $^1G_4$ level as shown in the RT PL spectra shown in Fig. 3. The observation of the red $^1G_4 \rightarrow {}^3F_4$ (~650 nm) and $^1G_4 \rightarrow {}^3H_5$ (~780 nm) transitions are clearly detected, which means that different Tm^{3+}-related emitting centres coexist in the same sample suggesting that the ions must be placed in different site symmetry. Also, with pumping within the $^1G_4$ multiplet and for the 1100–1800 nm spectral range, the $^1G_4 \rightarrow {}^3H_4$ (~1200 nm), $^3H_4 \rightarrow {}^3F_4$ (~1500 nm) and a transition nearby 1750 nm can be detected (Fig. 4a). At 8 K, and assuming that the emission originates from the lower energy crystal-field component of the excited $^1G_4$ state, a total 2J+1 = 9 lines are expected for the Tm^{3+} ions in low site symmetries (e.g. triclinic, monoclinic and rhombic) sites. Fig. 4b clearly evidences that the number of observed emission lines is also higher than the number expected

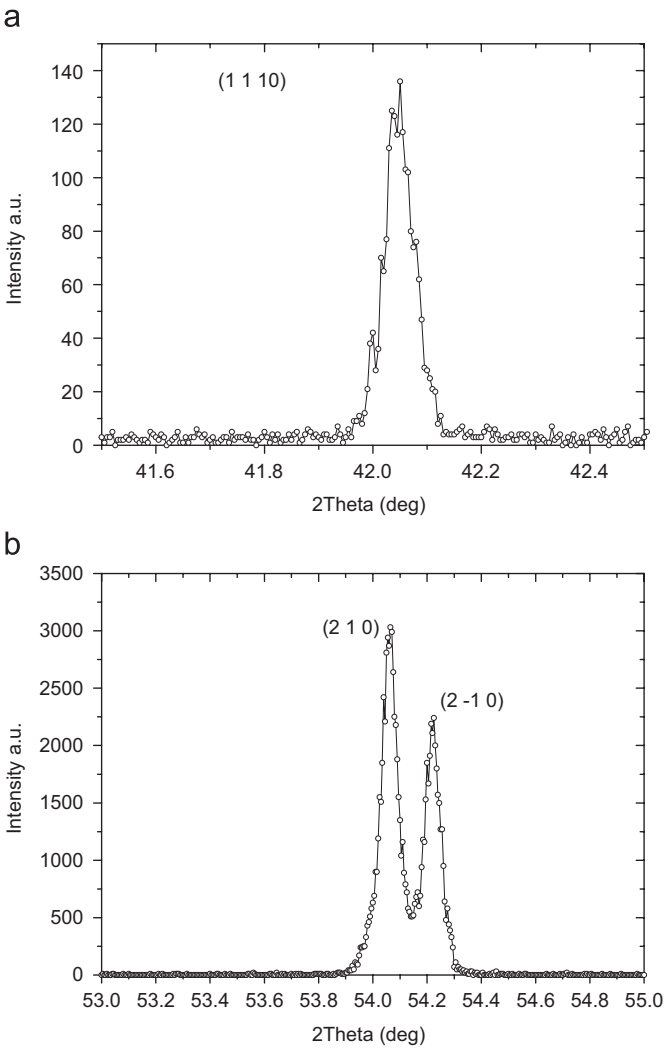

Fig. 1. (a) $2\theta-\theta$ scans for the (1 1 10) crystallographic plane. The same result was found for (1 $\bar{1}$ 10). The overlap of both planes confirms the monoclinic nature of samples. (b) $2\theta-\theta$ results for the (2 1 0) crystallographic planes family, indicating the presence of the triclinic phase due to splitting of the peaks.

for the Stark splitting in a single site with lowest symmetries. Remarkable is the absence of the recombination between the first and the ground state multiplets ($^3F_4 \rightarrow {}^3H_6$) that in several hosts occurs between 1600 and 2000 nm [5,10–12]. As for these wavelengths, we are in the limit of our spectral resolution; we are not able to warranty that low-energy transitions occur in that spectral region, which could be ascribed to the $^3F_4 \rightarrow {}^3H_6$ recombination. Nevertheless, from the temperature dependence of the PL spectra a thermally populated emission can be seen between 1600 and 1800 nm, which we tentatively assign to $^3F_4 \rightarrow {}^3H_6$ transition suggesting that efficient $Tm^{3+} \rightarrow Tm^{3+}$ energy transfer takes place via ground and/or excited state absorption. This assumption is also followed by the overall integrated intensity of the $^1G_4 \rightarrow {}^3H_4$ (~1200 nm) and $^3H_4 \rightarrow {}^3F_4$ (~1500 nm) which are seen to increase with temperature as observed in Fig. 4c.

Despite the dielectric properties, at microwave frequencies, are clearly dependent on material structure [13,14], as confirmed in Eu-doped Ta_2O_5 LHPG fibres [6], the Tm-doped LHPG fibres do not exhibit significant variation in dielectric constant, even though the transition is from monoclinic to triclinic. In fact, a value of $\varepsilon' = 21$ at 5 GHz was observed for undoped Ta_2O_5 sample, while the 0.1% and 1% Tm-doped samples exhibit 20 and 18,

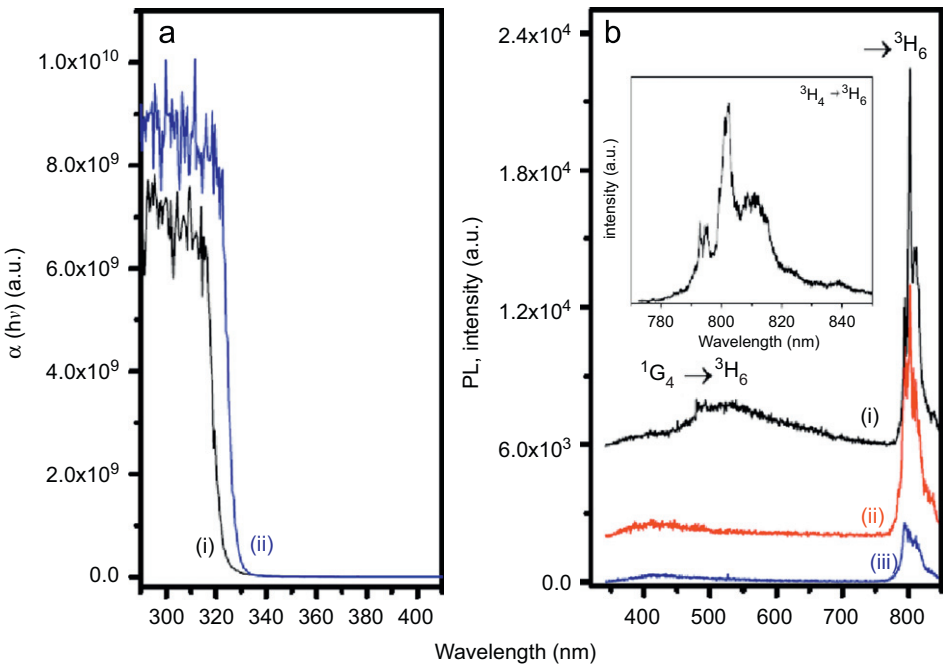

Fig. 2. (a) Absorption coefficient for the Ta_2O_5 undoped single crystalline fibre at (i) 14 K and (ii) RT. (b) Unpolarized 14 K (i), 140 K (ii) and RT (iii) PL spectra for the Ta_2O_5:Tm (1 at%) obtained with 325 nm excitation. Inset: expanded zone of the $^3H_4 \rightarrow {}^3H_6$ transition.

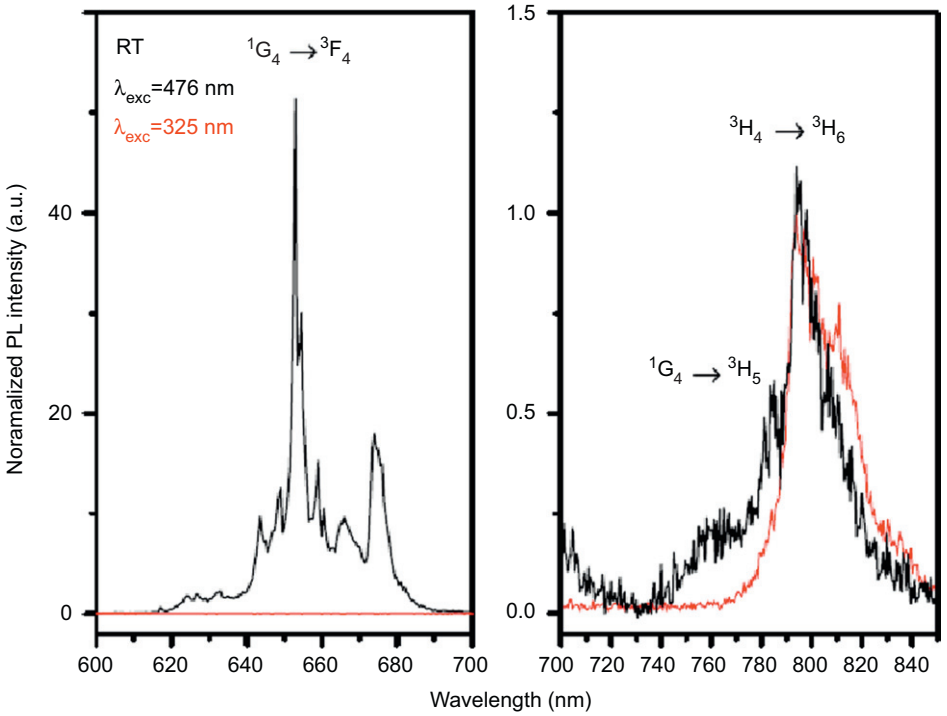

Fig. 3. Normalized RT PL spectra observed with above band-gap excitation (325 nm) and pumping resonantly (476 nm) into the $^1G_4$ level.

respectively. However, the dielectric losses maintain very low values in the order of 5×10^{-3}.

4. Conclusions

The incorporation of Tm^{3+} ions induces a structural transition in the Ta_2O_5 fibres. Samples doped with Tm^{3+} concentrations of 0.1 at% reveal a monoclinic structure, while the triclinic phase is observed for concentrations of the order of 1.0 at%.

From the PL data one observes Tm^{3+} optical activation for the highest-doped Ta_2O_5 LHPG fibre, which has predominantly triclinic crystal structure. Using the above band gap and resonant excitation into the $^1G_4$ level, we are able to identify different Tm^{3+}-related centres that must be correlated with different site symmetry. This conclusion can also be drawn from the observed Stark splittings. The observed number of lines suggests that both centres are in low site symmetries. Furthermore, efficient energy transfer between $Tm^{3+} \rightarrow Tm^{3+}$ ions must occur in order to explain the absence, at low temperatures, of the lowest energetic

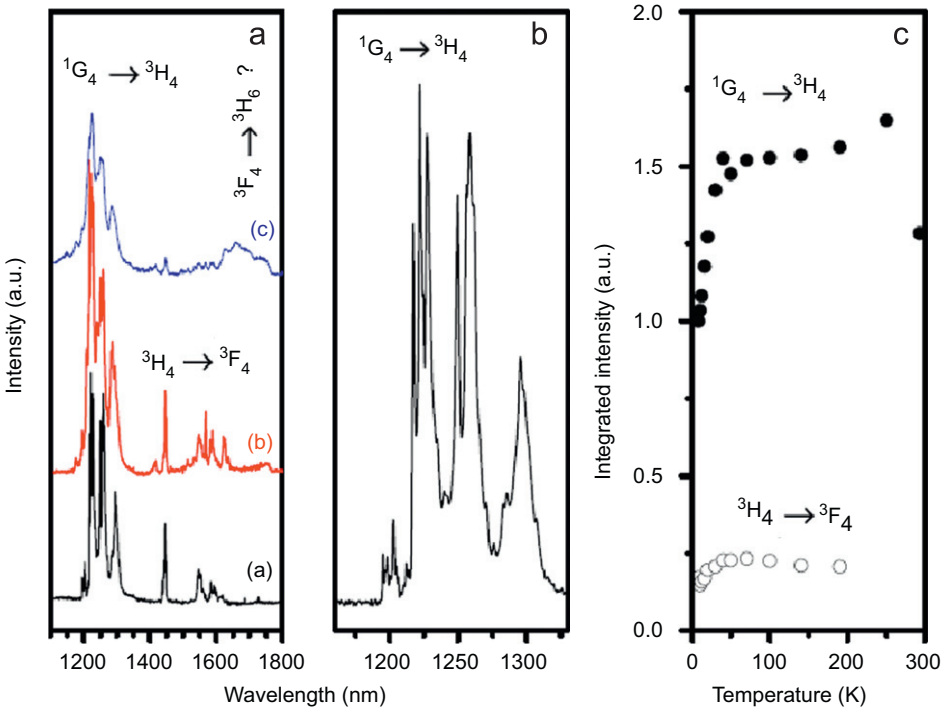

Fig. 4. Unpolarized PL spectra of the Ta_2O_5:Tm (1 at%) sample obtained with pumping in the $^1G_4$ energy level. (a) Temperature-dependent PL for selected temperatures (a) 8 K, (b) 140 K and (c) RT. (b) Enlarged 8 K PL spectrum of the $^1G_4 \rightarrow {}^3H_4$ transition. (c) Temperature dependence of the integrated PL intensity for $^1G_4 \rightarrow {}^3H_4$ (solid circles) and $^3H_4 \rightarrow {}^3F_4$ (open circles) transitions.

transition between the first and the ground state multiplets and the temperature dependence of the integrated intensity.

The dielectric constant is almost the same for the undoped and the doped materials, as well as the low dielectric losses, despite the phase transition that occurs with Tm doping.

Acknowledgments

M. Peres and C.P.L. Rubinger (BPD 34868/2007) thank UA and FCT for grants. The financial funding from the FCT Projects PTDC/CTM/66195/2006, PTDC/FIS/66262/2006 and PTDC/FIS/72843/2006 is also gratefully acknowledged.

References

[1] P.S. Dobal, R.S. Katiyar, Y. Jiang, R. Guo, A.S. Bhalla, J. Phys. Chem. Solids 61 (2000) 1805.
[2] G.L. Brennecka, D.A. Paune, P. Sarin, J.-M. Zuo, W.M. Kriven, J. Am. Ceram. Soc. 90 (2007) 2947.
[3] P.S. Dobal, R.S. Katiyar, Y. Jiang, R. Guo, A.S. Bhalla, J. Appl. Phys. 87 (2000) 8688.
[4] G.L. Brennecka, D.A. Payne, J. Am. Ceram. Soc. 89 (7) (2006) 2369.
[5] A.S.S. de Camargo, M.R.B. Andreeta, A.C. Hernandes, L.A.O. Nunes, Opt. Mater. 28 (2006) 551.
[6] C.P.L. Rubinger, L.C. Costa, M. Macatrão, M. Peres, T. Monteiro, F.M. Costa, N. Franco, E. Alves, B.Z. Saggioro, M.R.B. Andreeta, A.C. Hernandes, Appl. Phys. Lett. 92 (2008) 252904.
[7] C.P.L. Rubinger, L.C. Costa, Microwave Opt. Technol. Lett. 49 (2007) 1687.
[8] F. Henry, A. Berteaud, J. Microwave Power 15 (4) (1980) 65.
[9] W.T. Carnall, P.R. Fields, J. Morrison, R. Sarup, J. Chem. Phys. 52 (1970) 4054.
[10] T. Tsuboi, J. Electrochem. Soc. 147 (2000) 1997.
[11] M.C. Pujol, F. Guell, X. Mateos, Jna Gavaldà, R. Solé, J. Massons, M. Aguiló, F. Díaz, Phys. Rev. B 66 (2002) 144304.
[12] I. Sokólska, W. Ryba-Romanowski, S. Golab, M. Baba, M. Swirkowicz, T. Lukasiewicz, J. Phys. Chem. Solids 61 (2000) 1573.
[13] T. Lacrevaz, B. Flechet, A. Farcy, J. Torres, M. Gros-Jean, C. Bermond, O. Cueto, B. Blampey, G. Angenieux, J. Piquet, F. de Crecy, Microelectron. Eng. 82 (2005) 548.
[14] D. Makovec, J.M. Zuo, R. Twesten, D.A. Payne, J. Solid State Chem. 179 (2006) 1782.